Unraveling the Surface Reactivity of Pristine and Ti Doped Hematite with Water

Pierre-Marie Deleuze, Héléne Magnan, Antoine Barbier, Mathieu Silly, Bruno Domenichini, Céline Dupont

Unraveling the Surface Reactivity of Pristine and Ti Doped Hematite with Water

Pierre-Marie Deleuze,[†] Hélène Magnan,[‡] Antoine Barbier,[‡] Mathieu Silly,[¶] Bruno Domenichini,[†] and Céline Dupont[*,†]

[†]*Laboratoire Interdisciplinaire Carnot de Bourgogne (ICB), UMR 6303 CNRS, Université Bourgogne Franche-Comté, BP 47870, 21078 Dijon Cedex, France*

[‡]*Université Paris Saclay, CEA, CNRS, Service Physique Etat Condense (SPEC), F-91191 Gif Sur Yvette, France*

[¶]*Synchrotron SOLEIL, F-91192 St Aubin, France*

E-mail: celine.dupont@u-bourgogne.fr

Abstract

Water adsorption and dissociation on undoped and Ti doped hematite thin films were investigated using near ambient pressure photoemission and DFT calculations. A fine understanding of doping effects is of prime importance in the framework of photoanodes efficiency in aqueous conditions. By comparison to pure Fe_2O_3 surface, the Ti(2%)-Fe_2O_3 surface shows a lower hydroxylation level. We demonstrate that titanium induces wide structural modifications of the surface, preventing from reaching the full hydroxylation.

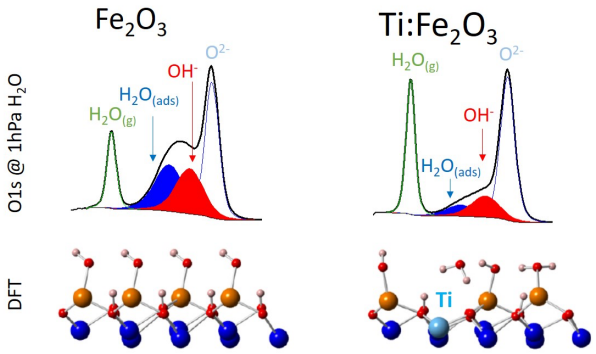

Increase of world population and evolution of society are responsible for an increasing global energy demand. Since 2001, the world annual energy consumption has increased by 25% to reach 16 TW. Without any effort, 30 TW should be needed in 2050.[1] Satisfying this additional energy demand using conventional production means would be highly detrimental to environment. It is thus mandatory to find an efficient solution for producing more and cleaner energy. Providing efficient harvest and use, solar energy can provide enough environment friendly resources to supply human energy demand. Fujishima and Honda[2] have evidenced the ability of TiO_2 for producing clean hydrogen through water photoelectrolysis induced by solar energy. However, despite a huge amount of research to improve the photoanode efficiency, no daily applications have emerged. Among all investigated materials, the early proposed hematite[3] is certainly one of the most promising candidates thanks to its suitable band-gap ($\sim$ 2.3 eV) allowing for the absorption of almost 40 % of the solar spectrum with a theoretical efficiency of 13%,[4] its high abundance, its stability towards corrosion and its non-toxicity.[5] However, α-Fe_2O_3 (named Fe_2O_3 in the following) also presents several drawbacks like a low conductivity and a high recombination rate harshly limiting its efficiency. Numerous options, such as doping,[6–8] nanostructuration[9–11] or coupling with a second metal-oxide,[12–14] have been proposed to improve hematite.

Among the different available dopants, titanium has been widely studied, and is certainly a promising route.[8,15–18] Most studies[19–22] about doped hematite have been devoted to understand the charge carrier dynamics and more particularly how dopants can slow down the electron / hole recombination, a key issue towards a better efficiency of hematite. Nevertheless, the presence of Ti - or any other dopant - does not only affect the electronic properties and as mentioned by Kronawitter[23] and coworkers, the increasing conductivity induced by the presence of Ti can not by itself explain efficiency improvements observed on doped hematite. Indeed, the presence of titanium doesn't only affect this electronic aspect but also likely plays a role on the structural and thermodynamic behavior of the water/hematite interface. In particular, by modifying the surface acidity and structure, the presence of tita-

nium can influence the interaction between water and hematite. If the latter has been widely investigated on pure hematite both experimentally[24–26] and theoretically,[27–30] such studies are rather scarce for Ti-doped hematite.[31] In particular, as far as we know the impact of the presence of Ti on the interaction of water and hematite has not been reported. Understanding the behavior at the interface between the photoanode and water is a key issue to improve these photocatalytic materials. In this framework, a deeper understanding at the atomistic level of mechanisms governing the interaction of water with pure and doped hematite is highly desirable. To do so, we propose to unravel the processes at the water/(Ti-)Fe_2O_3 interface thanks to NAP-XPS experiments combined to DFT calculations.

The NAP-XPS experiments were performed at the TEMPO beamline at synchrotron SOLEIL at room temperature. The samples (20 nm) - Fe_2O_3(0001) and Ti(2%)-Fe_2O_3(0001) were epitaxially grown on Pt(111) by atomic oxygen assisted molecular beam epitaxy.[8] Before XPS measurements, initial surfaces were annealed under molecular oxygen pressure (10^{-6} hPa) at 600K to regenerate clean and well-ordered surfaces before water exposure which was carried out in the 0.008 - 1.0 hPa range. O1s spectra were collected using a photon energy of 860 eV in order to record O1s line with kinetic energy close to 300 eV, i.e. being highly sensitive to the surface. The DFT calculations were performed under periodic boundary conditions (VASP 5.4.4[32,33]) with the Perdew-Burke-Ernzerhof exchange-correlation functional (PBE).[34] The electron-ion interaction was described within the projector-augmented plane-wave (PAW) method[35] with a kinetic energy cutoff of 550 eV. Eight valence electrons were explicitly treated for Fe ($3d^7 4s^1$), twelve for Ti ($3s^2 3p^6 4s^2 3d^2$), six for O ($2s^2 2p^4$) and one for H ($1s^1$). The DFT+U approach was adopted for the inclusion of the on-site Coulomb repulsion of both Fe and Ti 3d electrons using the Dudarev approach[36] with the effective parameter U_{eff}(Fe) = 4.3 eV and U_{eff}(Ti) = 3.5 eV. In agreement with previous studies,[24,26,28,37–39] we only considered the Fe-terminated surface modeled by a 18-layers symmetrical slab in an hexagonal cell with $a_{Fe_2O_3}$= 10.133 Å and a vacuum of 20 Å. For

doped hematite, two Fe atoms (over the 48 Fe atoms) were substituted by two Ti atoms - one close to the surface, the other at the bottom of the cell - in order to keep the antiferromagnetism in the whole cell. This leads to a global doping level of 4.2 % over the whole cell. However, for surface reactivity issues, only the top Ti plays a role bringing doping to an effective level 2.1 %, similar to the experimental one. The Brillouin zone was sampled with a 5×5×1 Monkhorst-Pack k-point mesh and structural optimization with respect to atomic coordinates was carried out until the forces converged below 0.01 eV/Å, with all atoms allowed to relax. The convergence threshold on total energy was set to 10^{-6} eV.

To resolve the interaction between water and hematite, either pure or doped, we follow the adsorption of water on both samples described above by NAP-XPS. The evolution of the O1s spectra recorded for water pressures ranging from 0 to 1 hPa is reported on Figure 1.

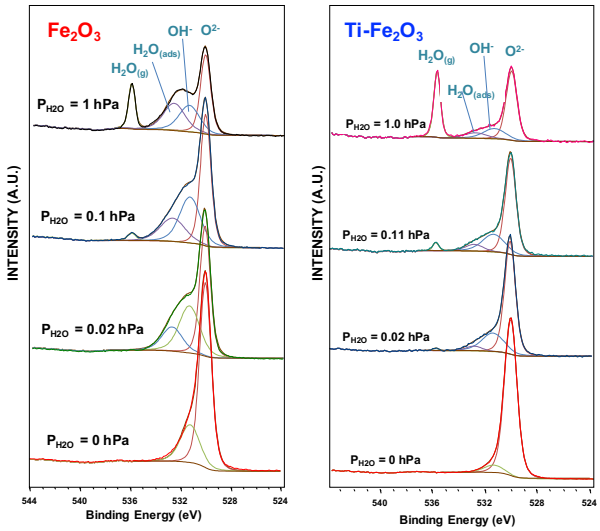

Figure 1: O1s photoemission spectra recorded at room temperature at a photon energy of 860 eV (left) on the $Fe_2O_3(0001)$ and (right) on the Ti-$Fe_2O_3(0001)$ surfaces. Spectra have been recorded under different pressures of H_2O ranging from (Bottom) 0 hPa to (Top) 1 hPa. Contributions of the different species, namely $H_2O_{(g)}$, $H_2O_{(ads)}$, OH^- and O_2^- are reported on each spectra.

For pure hematite, before water exposure, the main peak is centered at BE = 530.0 eV, with an additional contribution at BE = 531.5 eV which can be attributed to hydroxyl species adsorbed on the surface, in agreement with previous studies.[37] When P_{H_2O} increases,

the shoulder at higher energy also increases to lead to two components: a peak at BE=532.8 eV related to adsorbed molecular water on top of the hydroxylated hematite with a value similar to previous measurements[25,40] appears in addition to the OH contribution at BE = 531.5 eV. Starting from $P_{H_2O} = 0.1$ hPa, an additional contribution (536.0 eV) attributed to gas phase water starts to increase. Similar measurements have been performed on Ti(2%)-Fe_2O_3. Before water exposure, we still observe a peak at BE = 530.0 eV. However this peak is thinner than the one for pure hematite, with a very small contribution at 531.5 eV, indicating a lower initial hydroxylation in presence of Ti. At $P_{H_2O} = 0.02$ hPa, the maximum of hydroxylation is reached, as evidenced by the shoulder at 531.5 eV, which no longer increases for higher pressures. At this pressure, contrary to pure hematite the molecular adsorbed water contribution is almost negligible. At $P_{H_2O} = 0.11$ hPa, the peak associated to adsorbed water has slightly increased but remains lower than on pure hematite. Similarly to non-doped hematite, the contribution of gas phase H_2O appears at BE = 535.5 eV. Finally, at higher pressure ($P_{H_2O} = 1$ hPa), the comparison of pure and doped hematite indicates that a lower hydroxylation and water adsorption are obtained in presence of titanium.
To rationalize these observations, we compute the intensity ratio between the peak relative to hydroxyls and the one relative to oxygenated species and the intensity ratio between the peak relative to adsorbed molecular water and the one relative to oxygenated species, as a function of water pressure. Results are plotted on Figure 2 for both samples.

According to Figure 2 (Top), maximum of hydroxylation is reached for similar exposure ($P_{H_2O} \approx 0.063$ hPa) for both pure and doped hematite. However, as expected from analysis of Figure 1, a lower hydroxylation level with a ratio $OH^-/(O^{2-}+OH^-)$ equal to 0.26 is reached in presence of dopant, instead of 0.42 for pure hematite. Similarly in the presence of titanium, the evolution of adsorbed molecular water (Figure 2 (Bottom)) reaches a plateau for a 0.15 ratio at a pressure of 0.5 hPa. On the contrary for pure hematite, saturation in adsorbed molecular water doesn't seem to be reached at 1 hPa with a ratio close to 0.45. According to these results, the presence of titanium clearly modifies the interaction between

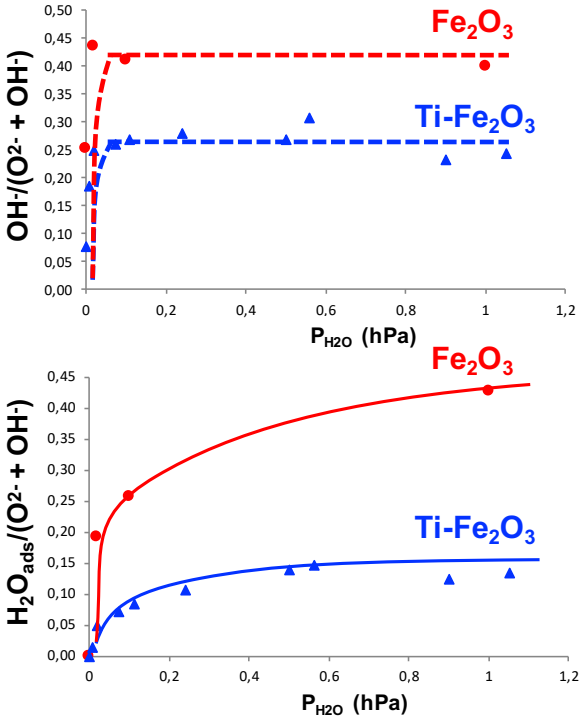

Figure 2: (Top) Evolution of the ratio of hydroxyl over oxygenated species as a function of H_2O pressure for $Fe_2O_3(0001)$ (red circles) and Ti-$Fe_2O_3(0001)$ (blue triangles). (Bottom) Evolution of the ratio of molecular adsorbed water over oxygenated species as a function of H_2O pressure for $Fe_2O_3(0001)$ (red circles) and Ti-$Fe_2O_3(0001)$ (blue triangles).

water and hematite.

To go deeper in the comprehension of mechanisms behind this modification, DFT calculations have also been performed. Starting from the Fe-terminated structure previously determined,[41] three cases of doping reported in SI have been considered, depending on the position of titanium relatively to the surface, introduced either in the first, second or third layer of hematite. The relative stability of these three cases has been studied for all possible positions of Ti in each layer (4 cases for the first layer and 8 cases for the second and third layers). Substitution of Fe by Ti in the first layer is in average 0.88 eV more stable than in the second layer and 0.16 eV than in the third one. Doping in the second layer can thus be excluded, while doping in the third one although less stable could be competitive. However, as we want to determine the influence of doping on the interface, in the following only doping in the first layer, namely close to the active site, will be considered, in agreement with previous studies.[42]

We started by studying the molecular and dissociative adsorption of water on pure and doped hematite. Given the experimental range of water pressures, we firstly considered the highest coverage of one monolayer, namely 4 equivalent of water molecules (either molecular or dissociated) per unit cell. Side views for the optimized structure for molecular adsorption of one monolayer of water on pure hematite are reported on Figure 3, while top views are given in SI. The four molecules present a similar adsorption geometry with a distance between the water molecule and the surface (d(Fe-O)) of 2.16 Å and the water molecule being tilted towards the surface thanks to an hydrogen bond of 1.65 Å. This leads to a global adsorption energy of -4.36 eV (see Table 1). These results are fully consistent with previous results of Nguyen *et al.*[27] The same calculations have been performed in presence of titanium. As reported on Figure 3, the four water molecules do not have the same behavior anymore. The three molecules associated with the three surface iron atoms present a tilted geometry close to the one observed on undoped hematite, with only small discrepancies. In particular d(Fe-O) is no longer equal for the three molecules but varies between 2.11 and 2.22 Å, as

well as hydrogen bonds ranging between 1.63 and 1.79 Å. On the contrary, the last molecule on top of titanium presents a completely different behavior, not even bonding to the surface (d(Ti-O) = 3.61 Å). This leads to an overall adsorption energy lower than without Ti: -3.87 eV instead of -4.36 eV. This discrepancy comes mainly from the non adsorption of water on top of Ti. However, besides the role of titanium - from preventing the adsorption of the fourth molecule, it is also important to determine how the presence of the dopant modifies the interaction of the three other molecules with the iron atoms. To do so, we optimized a system with only three adsorbed water molecules on top of the three iron surface atoms, for pure and doped hematite (see Table 1). The adsorption energies are very close: -3.43 eV and -3.37 eV, evidencing that when the water is adsorbed on iron sites, there is no influence of the neighbouring titanium. We can thus conclude that, at the adsorption level, the role of titanium is to lower the global coverage by removing an adsorption site. This is directly related to the surface structure of doped hematite as the titanium atom is relaxed inside the surface. Indeed, on bare doped hematite, Ti is 1.05 Å below the plane defined by the three surface iron atoms, being only 0.43 Å higher than the second layer. In the presence of water (Figure 3 (Top-Right)), Ti is even more inside the surface, being 1.20 Å below the plane defined by surface iron atoms. This clearly decreases the accessibility of the titanium and can thus explain the absence of water adsorption on this atom. Hence, from a purely thermodynamic point of view, the molecular adsorption rate is reduced by 25% in presence of Ti.

Table 1: Adsorption energies (in eV) for the molecular adsorption and the dissociative adsorption of four and three water molecules on pure and doped hematite. The reaction energy of the dissociation of four water molecules, namely ΔE_{disso} = E_{ads}(4(OH+H))-E_{ads}($4H_2O$) is also reported.

	α-Fe_2O_3	α-(Ti)Fe_2O_3
E_{ads}($4H_2O$)	-4.36	-3.87
E_{ads}(4(OH+H))	-5.05	-4.71
ΔE_{disso}($4H_2O \rightarrow$4(OH+H))	-0.68	-0.84
E_{ads}($3H_2O$)	-3.43	-3.37
E_{ads}(3(OH+H))	-3.55	-3.49

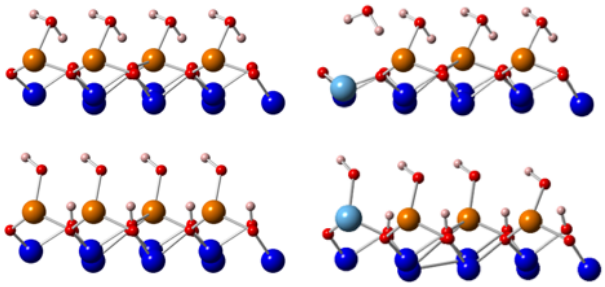

Figure 3: Side views of (Top) molecular adsorption and (Bottom) dissociative adsorption of a monolayer of water on (Left) Fe_2O_3 (Right) Ti-Fe_2O_3. Red spheres correspond to O atoms, light blue ones to titanium, white ones to hydrogen, while dark blue and golden yellow spheres denote Fe atoms. The two different colors of Fe atoms stand for their different magnetism to respect the antiferromagnetic ordering of hematite.

We then investigated the discrepancy for hydroxylation level by computing the dissociative adsorption of water. Side views and relative energies of optimized structures are reported on Figure 3 and Table 1, respectively, while top views are given in SI. Contrary to molecular adsorption, both pure and doped hematite present very similar structures. In absence of titanium the four hydroxyls are completely equivalent with d(Fe-O) = 1.83 Å, while titanium induces a slight increase of the bonds to lead to values for d(Fe-O) comprise between 1.84 and 1.88 Å and d(Ti-O) = 1.85 Å. This results in a lower adsorption energy on the doped surface with E_{ads}(4(OH+H)) = -4.71 eV instead of -5.05 eV for pure hematite. The lower difference between the two surfaces observed for dissociative adsorption compared to molecular adsorption can be explained by the difference of geometry between molecular and dissociated water, removing the geometrical issues of titanium accessibility. With this in mind the difference in energy might come only from the difference of interaction of the OH fragment on Ti compared to Fe. To check on this, dissociative adsorption of three water molecules on the three iron surface atoms of doped hematite has been studied and compared to the same coverage on pure hematite, with values reported on Table 1. We thus obtained similar values on both surfaces with an adsorption energy, E_{ads}(3(OH+H)), of -3.55 eV on pure hematite, similar to the -3.49 eV calculated in presence of dopant. This confirms that the difference observed for the four molecules only comes from the difference of interaction

between OH and Ti, the other sites not being affected by the neighbouring titanium.

Finally the reaction energy of dissociation has been evaluated on both surfaces, leading to exothermic reactions, with values of -0.68 and -0.84 eV for pure and doped hematite, respectively. One can mention that the dissociation is thermodynamically slightly more favorable in presence of titanium. This is directly related to results reported above, namely the fact that the presence of titanium has larger influence on the molecular than on the dissociative state. According to these results the full hydroxylation is thus thermodynamically favorable on both surfaces. However to assure the decomposition, the reaction should also be kinetically favorable. To evaluate this point one should calculate the activation energy barriers of all elementary steps from molecular adsorption to dissociative adsorption of a complete monolayer. To do so, formation of the full hydroxylated surface from molecular adsorption has been decomposed in four elementary steps on both pure and doped hematite, with each elementary step studied through Nudged Elastic Band (NEB) calculations.[43] The case of pure hematite is firstly studied with energy profile reported on Figure 4 while corresponding structures are reported on Figure 5 and in SI. As mentioned previously, the whole

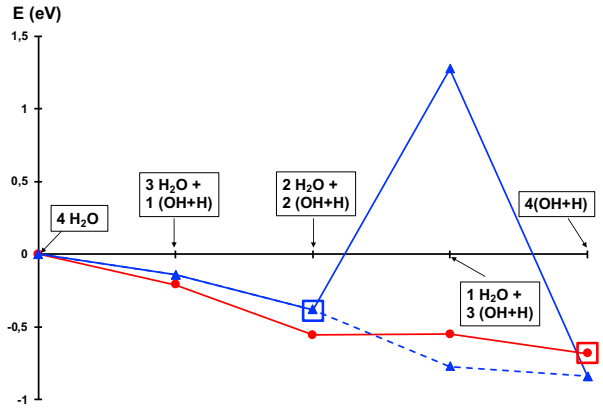

Figure 4: Energy profiles for the dissociation of 4 water molecules on Fe_2O_3 (red circles) and on Ti-Fe_2O_3 (blue triangles - plain and dashed lines). The energy reference is the molecular adsorption of 4 water molecules on each surface. Red and blue squares indicate effective final state for pure and doped hematite, respectively.

pathway is exothermic, with only the third dissociation being almost athermic. According to NEB calculations, all these elementary steps occur without any activation energy leading

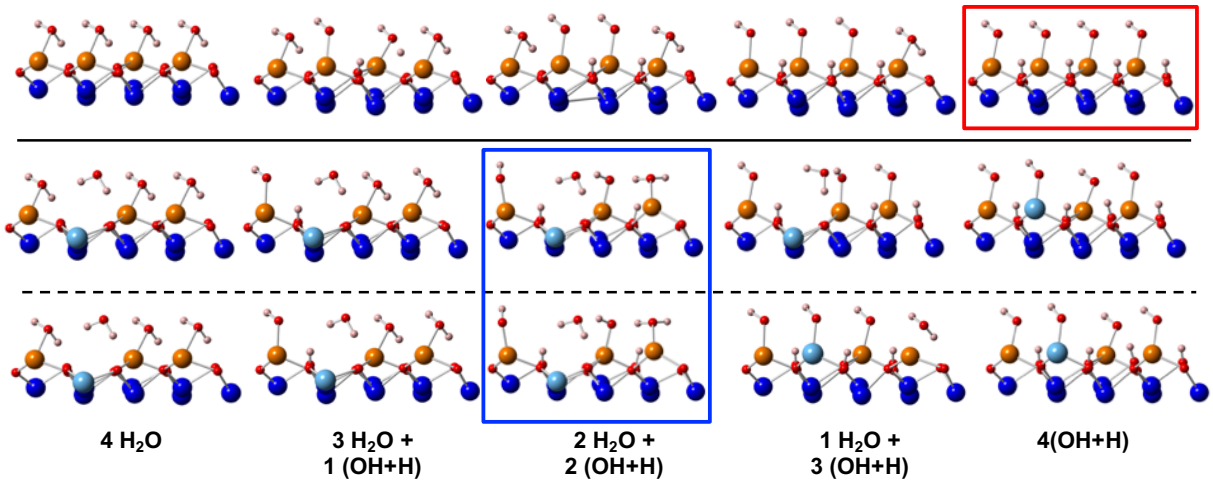

Figure 5: Side views of the different intermediate states for the decomposition of 4 water molecules on (Top) Fe_2O_3, (Middle) Ti-Fe_2O_3 - Path 1 and (Bottom) Ti-Fe_2O_3 - Path 2. For sake of clarity only the two topmost layers are reported. Red spheres correspond to O atoms, light blue ones to titanium, white ones to hydrogen, while dark blue and golden yellow spheres denote Fe atoms. The two different colors of Fe atoms stand for their different magnetism to respect the antiferromagnetic ordering of hematite. Effective final states for pure and doped hematite are highlighted by red and blue boxes, respectively.

to a spontaneous dissociation and thus spontaneous full hydroxylation. This is in agreement with previous results of Nguyen *et al.*[27] where a 0.06 eV barrier - easily compensated by ZPE - has been calculated. This result directly stems from the geometries. Indeed, in the initial state water molecules are tilted towards the surface thanks to hydrogen bonds. This leads to an elongation - and thus a weakening of the O-H bond facing the surface to 1.04 Å. After the dissociation of the first molecule, this phenomenon is even more engaged for the molecule adsorbed diagonally compared to the dissociated one, as its O-H bond facing the surface now reachs 1.07 Å. The last two dissociations then occur according to the same pattern.

Concerning the doped systems, picture differs. First of all, due to the presence of a Ti atom on the surface, this latter gets deprived of some symmetry. Hence, depending on which step of the decomposition occurs on titanium several pathways (12) are possible. These pathways can be summarized in two scenarii, named Path 1 and Path 2 in the following, for which the energy profiles are reported in blue plain and dashed lines, respectively on Figure 4, with

corresponding structures on Figure 5 and in SI.

Firstly, as already mentioned, the whole decomposition is exothermic. However this is not the case for each elementary steps of Path 1: indeed, the third step is widely endothermic with a reaction energy of 1.64 eV. Hence even though, according to NEB calculations all other elementary steps do not present any activation energy, as on pure hematite, the endothermicity of this third step prevent to get an accessible transition state and thus to reach the full hydroxylation. This can be directly interpreted in terms of structures. Indeed, the second dissociation induces some modifications on the two remaining water molecules. The one on top of titanium moves slightly away from the surface with an increase of d(Ti-O) from 3.63 Å to 3.75 Å, while the main modification occurs on the water molecule still molecularly adsorbed on a Fe atom. Due to dissociation of other molecules on the two iron atoms around this site, the third water molecule straightens up, its plane becoming perfectly parallel to the surface. As a consequence there is no more hydrogen bond with the surface to weaken one of the bonds of the water molecule. This situation can be directly ascribed to the non adsorbed water molecule inducing some strains at the interface, as no such phenomenon occurs on pure hematite.

The thermodynamics of Path 2 - dashed line on Figure 4 - are similar to undoped hematite with all elementary steps being exothermic. Still similarly to undoped hematite, the two first steps, in which titanium is not involved, occur without any activation energy. On the other hand, nudged elastic band calculations did not enable to identify a suitable transition state for the third dissociation occurring on top of the titanium. Again the structure can be directly incriminated. Indeed as can be seen on Figure 5, in the second intermediate, namely $2H_2O$ + 2(OH+H), titanium is still inside the surface being only 0.37 Å beyond the second layer but 1.47 Å below the first layer. This atom is thus unattainable preventing the dissociation of the third water molecule on its top. As a consequence, as for Path 1, the third dissociation is kinetically forbidden due to the structure induced by the presence of titanium. While the full hydroxylation is spontaneously reached on hematite, only two water molecules

can dissociate on Ti-Fe_2O_3, the third dissociation being kinetically prohibited. This result is in good agreement with the 0.26 ratio for hydroxyl species measured experimentally on doped hematite, compared to the value of 0.42 observed on undoped hematite.

In conclusion, synchrotron NAP-XPS experiments combined to DFT calculations have allowed to unravel the role of Ti on the water/hematite interface. The strong structural surface modifications induced by the presence of titanium thermodynamically reduce the molecular adsorption of water by 25 % and kinetically prevent the water dissociation beyond half a monolayer.

Acknowledgement

The authors thank Dr. Jean-Jacques Gallet for the NAP equipment. Calculations were performed using HPC resources from DNUM CCUB (Centre de Calcul de l'Université de Bourgogne). This work was also granted access to the HPC resources of IDRIS under the allocation 2020-A0090811108 made by GENCI. The authors also thanks the ANR for financial support through projects ANR-15-CE05-PHOTO-POT and ANR-17-EURE-0002 (EIPHI Graduate School).

Supporting Information Available

The Supporting Information contains the lateral views for detailed structures of the four cases of doping, the top views of molecular and dissociative adsorption of a monolayer of water on pure and doped hematite and the top views for all intermediate states of the decomposition of four water molecules on pure and doped hematite.

References

(1) Vesborg, P.; Jaramillo, T. Addressing the Terawatt Challenge: Scalability in the Supply of Chemical Elements for Renewable Energy. *RSC Adv.* **2012**, *2*, 7933–7947.

(2) Fujishima, A.; Honda, K. Electrochemical Photolysis of Water at a Semiconductor Electrode. *Nature* **1972**, *238*, 37–38.

(3) Hardee, K.; Bard, A. Semiconductor Electrodes. V. The Application of Chemically Vapor Deposited Iron Oxide Films to Photosensitized Electrolysis. *J. Electrochem. Soc.* **1976**, *123*, 1024–1026.

(4) Van de Krol, R.; Liang, Y.; Schoonman, J. Solar Hydrogen Production with Nanostructured Metal Oxides. *J. Mater. Chem.* **2008**, *18*, 2311–2320.

(5) Sivula, K.; Formal, F. L.; Grätzel, M. Solar Water Splitting: Progress Using Hematite (α-Fe_2O_3) Photoelectrodes. *Chem. Sus. Chem.* **2011**, *4*, 432–449.

(6) Hu, Y.-S.; Kleiman-Shwarsctein, A.; Forman, A. J.; Hazen, D.; Park, J.-N.; McFarland, E. W. Pt-Doped α-Fe_2O_3 Thin Films Active for Photoelectrochemical Water Splitting. *Chem. Mater.* **2008**, *20*, 3803–3805.

(7) Kleiman-Shwarsctein, A.; Hu, Y.-S.; Forman, A. J.; Stucky, G. D.; McFarland, E. W. Electrodeposition of α-Fe_2O_3 Doped with Mo or Cr as Photoanodes for Photocatalytic Water Splitting. *J. Phys. Chem. C* **2008**, *112*, 15900–15907.

(8) Magnan, H.; Stanescu, D.; Rioult, M.; Fonda, E.; Barbier, A. Enhanced Photoanode Properties of Epitaxial Ti Doped α-Fe_2O_3(0001) Thin Films. *Appl. Phys. Lett.* **2012**, *101*, 133908/1–133908/4.

(9) Mohapatra, S. K.; John, S. E.; Banerjee, S.; Misra, M. Water Photooxidation by Smooth and Ultrathin α-Fe_2O_3 Nanotube Arrays. *Chem. Mater.* **2009**, *21*, 3048–3055.

(10) Ling, Y.; Wang, G.; Wheeler, D. A.; Zhang, J. Z.; Li, Y. Sn-Doped Hematite Nanostructures for Photoelectrochemical Water Splitting. *Nano Lett.* **2011**, *11*, 2119–2125.

(11) Kay, A.; Cesar, I.; Grätzel, M. New Benchmark for Water Photooxidation by Nanostructured α-Fe_2O_3 Films. *J. Am. Chem. Soc.* **2006**, *128*, 15714–15721.

(12) Kronawitter, C. X.; Vayssieres, L.; Shen, S.; Guo, L.; Wheeler, D. A.; Zhang, J. Z.; Antoun, B. R.; Mao, S. S. A Perspective on Solar-Driven Water Splitting with All-Oxide Hetero-Nanostructures. *Energy Environ. Sci.* **2011**, *4*, 3889–3899.

(13) Yang, X.; Liu, R.; Du, C.; Dai, P.; Zheng, Z.; Wang, D. Improving Hematite-based Photoelectrochemical Water Splitting with Ultrathin TiO_2 by Atomic Layer Deposition. *ACS Appl. Mater. Interfaces* **2014**, *6*, 12005–12011.

(14) Neufeld, O.; Yatom, N.; Caspary Toroker, M. A First-Principles Study on the Role of an Al_2O_3 Overlayer on Fe_2O_3 or Water Splitting. *ACS Catalysis* **2015**, *5*, 7237–7243.

(15) Meng, X.; Qin, G.; Li, S.; Wen, X.; Ren, Y.; Pei, W.; Zuo, L. Enhanced Photoelectrochemical Activity for Cu and Ti Doped Hematite: The First Principles Calculations. *Appl. Phys. Lett.* **2011**, *98*, 112104/1–112104/3.

(16) Xie, J.; Yang, P.; Liang, X.; Xiong, J. Self-Improvement of Ti:Fe_2O_3 Photoanodes: Photoelectrocatalysis Improvement after Long-Term Stability Testing in Alkaline Electrolyte. *ACS Appl. Energy Mater.* **2018**, *1*, 2769–2775.

(17) Zhang, X.; Wang, X.; Yi, X.; Ye, J.; Wang, D. Alkali Treatment for Enhanced Photoelectrochemical Water Oxidation on Hematite Photoanode. *ACS Sustainable Chem. Eng.* **2019**, *7*, 5420–5429.

(18) Feng, F.; Li, C.; Jian, J.; Li, F.; Xu, Y.; Wang, H.; Jia, L. Gradient Ti-doping in hematite photoanodes for enhanced photoelectrochemical performance. *J. Power Sources* **2020**, *449*, 227473–227481.

(19) Barroso, M.; Pendlebury, S.; Cowan, A.; Durrant, J. Charge Carrier Trapping, Recombination and Transfer in Hematite (α-Fe_2O_3) Water Splitting Photoanodes. *Chem. Sci.* **2013**, *4*, 2724–2734.

(20) Klahr, B.; Hamann, T. Water Oxidation on Hematite Photoelectrodes: Insight into the Nature of Surface States through In Situ Spectroelectrochemistry. *J. Phys. Chem. C* **2014**, *118*, 10393–10399.

(21) Shavorskiy, A.; Ye, X.; Karslioglu, O.; Poletayev, A.; Hartl, M.; Zegkinoglou, I.; Trotochaud, L.; Nemsak, S.; Schneider, C.; Crumlin, E.; Axnanda, S.; Liu, Z.; Ross, P.; Chueh, W.; Bluhm, H. Direct Mapping of Band Positions in Doped and Undoped Hematite during Photoelectrochemical Water Splitting. *J. Phys. Chem. Lett.* **2017**, *8*, 5579–5586.

(22) Rodriguez-Gutierrez, I.; Souza Junior, J.; Leite, E.; Vayssieres, L.; Souza, F. An Intensity Modulated Photocurrent Spectroscopy Study of the Role of Titanium in Thick Hematite Photoanodes. *Appl. Phys. Lett.* **2021**, *119*, 071602–071608.

(23) Kronawitter, C.; Zegkinoglou, I.; Shen, S.-H.; Liao, P.; Cho, I.; Zandi, O.; Liu, Y.-S.; Lashgari, K.; Westin, G.; Guo, J.-H.; Himpsel, F.; Carter, E. A.; Zheng, X.; Hamann, T. W.; Koel, B. E.; Mao, S.; Vayssieres, L. Titanium Incorporation into Hematite Photoelectrodes: Theoretical Considerations and Experimental Observations. *Energy Environ. Sci.* **2014**, *7*, 3100–3121.

(24) Trainor, T.; Chaka, A.; Eng, P.; Newville, M.; Waychunas, G.; Catalano, J.; Brown Jr., G. Structure and Reactivity of the Hydrated Hematite (0001) Surface. *Surf. Sci.* **2004**, *573*, 204–224.

(25) Yamamoto, S.; Kendelewicz, T.; Newberg, J.; Ketteler, G.; Starr, D.; Mysak, E.; Andersson, K.; Ogasawara, H.; Bluhm, H.; Salmeron, M.; G.E. Brown, J.; Nilsson, A.

Water Adsorption on α-Fe_2O_3(0001) at Near Ambient Conditions. *J. Phys. Chem. C* **2010**, *114*, 2256–2266.

(26) Noh, J.; Li, H.; Osman, O.; Aziz, S.; Winget, P.; Bredas, J. Impact of Hydroxylation and Hydration on the Reactivity of α-Fe_2O_3 (0001) and (1102) Surfaces under Environmental and Electrochemical Conditions. *Adv. Energy Mater.* **2018**, *8*, 1800545/1–1800545/13.

(27) Nguyen, M.-T.; Seriani, N.; Gebauer, R. Water Adsorption and Dissociation on α-Fe_2O_3(0001): PBE+U Calculations. *J. Chem. Phys.* **2013**, *138*, 194709/1–194709/8.

(28) Ovcharenko, R.; Voloshina, E.; Sauer, J. Water Adsorption and O-defect Formation on Fe_2O_3(0001) Surfaces. *Phys. Chem. Chem. Phys.* **2016**, *18*, 25560–25568.

(29) Negreiros, F.; Pedroza, L.; Dalpian, G. Effect of Charges on the Interaction of a Water Molecule with the Fe_2O_3(0001) Surface. *J. Phys. Chem. C* **2016**, *120*, 11918–11925.

(30) Mahmoud, A.; Dupont, C. Enhancing α-Fe_2O_3(0001) Surfaces Reactivity through Lattice-Strain Control. *App. Surf. Sci.* **2020**, *534*, 147605–147611.

(31) Toroker, M. C. Theoretical Insights into the Mechanism of Water Oxidation on Nonstoichiometric and Titanium-Doped Fe_2O_3(0001). *J. Phys. Chem. C* **2014**, *118*, 23162–23167.

(32) Kresse, G.; Furthmüller, J. Efficiency of ab-initio Total Energy Calculations for Metals and Semiconductors using a Plane-Wave Basis Set. *Comput. Mater. Sci.* **1996**, *6*, 15–50.

(33) Kresse, G.; Furthmüller, J. Efficient Iterative Schemes for ab initio Total-Energy Calculations using a Plane-Wave Basis Set. *Phys. Rev. B* **1996**, *54*, 11169–11186.

(34) Perdew, J.; Burke, K.; Ernzerhof, M. Generalized Gradient Approximation Made Simple. *Phys. Rev. Lett.* **1996**, *77*, 3865–3868.

(35) Kresse, G.; Joubert, D. From Ultrasoft Pseudopotentials to the Projector Augmented-Wave Method. *Phys. Rev. B* **1999**, *59*, 1758–1775.

(36) Dudarev, S. L.; Botton, G. A.; Savrasov, S. Y.; Humphreys, C. J.; Sutton, A. P. Electron-Energy-Loss Spectra and the Structural Stability of Nickel Oxide: An LSDA+U study. *Phys. Rev. B* **1998**, *57*, 1505–1509.

(37) Thevuthasan, S.; Kim, Y.; Yi, S.; Chambers, S.; Morais, J.; Denecke, R.; Fadley, C.; Liu, P.; Kendelewicz, T.; Brown, G. Surface Structure of MBE-grown α-Fe_2O_3(0001) by Intermediate-Energy X-ray Photoelectron Diffraction. *Surf. Sci.* **1999**, *425*, 276 – 286.

(38) Lübbe, M.; Moritz, W. A LEED Analysis of the Clean Surfaces of α-Fe_2O_3(0001) and α-Cr_2O_3(0001) Bulk Single Crystals. *J. Phys.: Condens. Matter* **2009**, *21*, 134010/1–134010/8.

(39) Qiao, B.; Wang, A.; Yang, X.; Allard, L.; Jiang, Z.; Cui, Y.; Liu, J.; Li, J.; Zhang, T. Single-Atom Catalysis of CO Oxidation using Pt_1/FeO_x. *Nat. Chem.* **2011**, *3*, 634–641.

(40) Herman, G.; McDaniel, E.; Joyce, S. Interaction of D_2O with the Fe_3O_4(111) and the Biphase Ordered Structures on α-Fe_2O_3(0001). *J. Electron Spectrosc. Relat. Phenom.* **1999**, *101*, 433–438.

(41) Mahmoud, A.; Deleuze, P.; Dupont, C. The Nature of the Pt(111)/α-Fe_2O_3(0001) Interfaces Revealed by DFT Calculations. *J. Chem. Phys.* **2018**, *148*, 204701/1–204701/8.

(42) Liao, P.; Keith, J. A.; Carter, E. A. Water Oxidation on Pure and Doped Hematite (0001) Surfaces: Prediction of Co and Ni as Effective Dopants for Electrocatalysis. *J. Am. Chem. Soc.* **2012**, *134*, 13296–13309.

(43) Henkelman, G.; Uberuaga, B.; Jonsson, H. A Climbing Image Nudged Elastic Band

Method for Finding Saddle Points and Minimum Energy Paths. *J. Chem. Phys.* **2000**, *113*, 9901–9904.